Cryogenics 50 (2010) 158–166

Contents lists available at ScienceDirect

Cryogenics

journal homepage: www.elsevier.com/locate/cryogenics

CFD model of ITER CICC. Part VI: Heat and mass transfer between cable region and central channel

R. Zanino *, S. Giors, L. Savoldi Richard

Dipartimento di Energetica, Politecnico, Torino, Italy

ARTICLE INFO

Article history:
Received 16 January 2009
Received in revised form 26 October 2009
Accepted 28 November 2009

Keywords:
ITER
Superconducting magnets
Cable-in-conduit conductors
CFD
Friction factor
Heat transfer coefficient

ABSTRACT

Dual-channel cable-in-conduit conductors (CICC) are used in the superconducting magnets for the International Thermonuclear Experimental Reactor (ITER). As the CICC axial/transverse size ratio is typically ~1000, 1D axial models are customarily used for the CICC, but they require constitutive relations for the transverse fluxes. A novel approach, based on Computational Fluid Dynamics (CFD), was recently proposed by these authors to understand the complex transverse thermal–hydraulic processes in an ITER CICC from first principles. Multidimensional (2D, 3D) Reynolds-Averaged Navier–Stokes models implemented in the commercial CFD code FLUENT were validated against compact heat exchanger and ITER-relevant experimental data, and applied to *compute* the friction factor and the heat transfer coefficient in fully turbulent spiral rib-roughened pipes, mimicking the central channel of an ITER CICC. That analysis is extended here to the problem of heat and mass transfer through the perforated spiral separating the central channel from the cable bundle region, by combining the previously developed central channel model with a porous medium model for the cable region. The resulting 2D model is used to analyze several key features of the transport processes occurring between the two regions including the relation between transverse mass transfer and transverse pressure drop, the influence of transverse mass transfer on axial pressure drop, and the heat transfer coefficient between central channel and annular cable bundle region.

1. Introduction

Multi-channel cable-in-conduit conductors (CICC), see Fig. 1, will be used in the superconducting magnets for the International Thermonuclear Experimental Reactor (ITER) [1]. Supercritical helium (SHe) coolant flows both in the annular region, where the cable bundle is present, and in the central channel, delimited by a (perforated) spiral.

As the CICC axial/transverse size ratio is typically $\geqslant 10^3$ in a coil, 1D (axial) models [2], or combinations thereof [3,4] to approximately treat the actually multi-dimensional situation, are customarily used for the sake of sparing CPU time, but they require constitutive relations for the transverse fluxes, including friction factors and heat transfer coefficients.

Unfortunately, however, the wide database available at present on, e.g., friction factors, is neither fully comprehensive nor free of contradictions/ambiguities [5–7].

Therefore, a novel approach, based on Computational Fluid Dynamics (CFD), was recently proposed [7–11] to improve our understanding of the complex *local* transverse thermal–hydraulic processes in an ITER CICC and obtain transverse constitutive relations to feed the *global* 1D codes. So far our modeling was mainly restricted to the central channel region, with the only exception of a study of friction in the simplest possible cable bundle, made of a single triplet [10].

In particular, 2D and 3D simulations were used in [7] to confirm that the 2-layer k–ε turbulence model [12] is the most suitable for the separated flow problems relevant in the central channel case, where detachment occurs at the leading edge of the spiral and reattachment of the flow may occur in the gap, depending on the gap width over height (g/h) ratio. The influence of the different geometrical parameters (g, h, central channel diameter) on friction was studied in [8], with particular reference to the dependence on g/h and to synergistic effects. For the ITER CS and TF relevant 7 mm/9 mm (ID/OD) central channel, a correlation was developed in [9] based on the results of our computational experiments, predicting a lower pressure drop than the present ITER design criteria, for a given total mass flow rate. Finally, in [11] the Colburn analogy between friction and heat transfer was shown *not* to be verified in the case of the CICC central channel and the computed heat transfer coefficient *on the central channel side* turned out to be not much larger than the smooth-pipe Dittus–Boelter value.

* Corresponding author.
E-mail address: roberto.zanino@polito.it (R. Zanino).

0011-2275/$ - see front matter © 2009 Elsevier Ltd. All rights reserved.
doi:10.1016/j.cryogenics.2009.11.005

Nomenclature

dm/dt, $\dot{m}$	mass flow rate
f	friction factor
g	spiral gap width
h	spiral thickness
k	turbulent kinetic energy
pt	spiral pitch
p	pressure
$\tilde{p}$	pressure modulation
r	radial coordinate
v	flow velocity
v_{mag}	velocity magnitude
w	axial width of the spiral
x	spatial coordinate along conductor axis
A	cross section
C_p	specific heat at constant pressure
D_{in}	inner diameter of the central channel
D_{Jk}	diameter of the cable region (inner diameter of the jacket)
H	heat transfer coefficient
J	inertial constant
K	permeability
L	length along conductor
NP	non periodic model
Nu	Nusselt number
Q	heat source
P	periodic model
Re	Reynolds number
S	porous medium source term in momentum Navier–Stokes equations
SHe	supercritical helium
T	temperature

Greeks

δ_{ij}	Kronecker delta
ε	turbulent dissipation rate
μ	viscosity
ρ	density
θ	normalized temperature
ϕ	arbitrary scalar quantity
Γ	radial mass flux
Δp	pressure difference
$\langle \Delta p \rangle$	volume averaged pressure difference
$\langle \Delta p_0 \rangle$	volume averaged pressure difference obtained from the periodic model

Subscripts

B	bundle
H	central channel (hole)
n	unit vector perpendicular to the control surface
r	radial component
B→H	bundle to hole
In	inlet
Jk	jacket
Out	outlet
tot	total
$\perp$	transverse

The commercial CFD code FLUENT was used for all of these studies and the results of the code were validated showing good agreement against experimental data in many different (2D and 3D) geometries: the computed friction factor in the central channel f_H turned out to be within ~±15% error bar from the measured values, while the computed Nusselt number on the central channel side Nu_{H} resulted within ~±30% error bar from the measured values.

Fig. 1. A typical ITER CICC (top) and the spiral delimiting its central channel (bottom).

Here we extend the approach developed in the previous papers of this series by including two substantially new features: (1) the annular cable region, treated as a porous model, so that the entire CICC cross section available for the SHe flow is now treated by the model; (2) the perforation of the spiral delimiting the central channel, so that mass transfer is now allowed between the two CICC regions. Inclusion of a net mass transfer through the spiral has also a major implication, i.e., the impossibility to assume a periodic model in the axial direction as done so far, see below.

2. Model equations and boundary conditions

The commercial CFD code FLUENT is used in this paper, assuming azimuthal symmetry, i.e., a 2D (axial/radial) cylindrical geometry, which was shown in the past [7–9] to be a very good approximation of the real 3D geometry of an ITER CICC. The entire cross section of the CICC is modeled, see Fig. 1, and the geometrical data used in the simulation are listed in Table I, where g is the gap size, h is the spiral thickness, w is the spiral (axial) width, $pt = g + w$ is the spiral pitch, D_{in} is the inner diameter of the central channel and D_{Jk} is the diameter of the cable region (inner diameter of the jacket).

For the central channel the same model as in the previous papers of this series is used, i.e., the Reynolds-Averaged Navier–Stokes (RANS) with 2-layer k–ε model as turbulence closure.

The bundle region is treated as a porous medium by adding the following source term to the i-th component of the Navier/Stokes momentum equations:

$$S_i = -\left(\sum_{j=1}^{3} D_{ij}\mu v_j + \sum_{j=1}^{3} C_{ij}\frac{1}{2}\rho v_{mag} v_j\right) \quad (1)$$

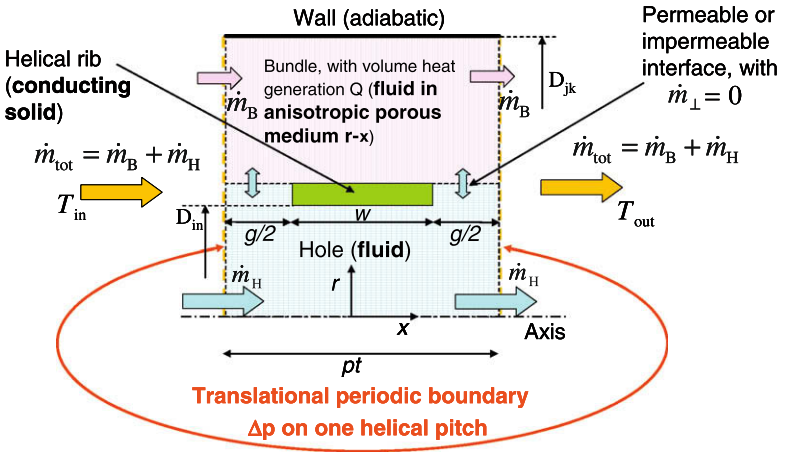

Fig. 2. Structure of the periodic model. A single pitch length of the spiral is considered in this case.

The first term on the rhs of Eq. (1) is the Darcy contribution, while the second is the inertial (Forchheimer) contribution, v_{mag} being the velocity magnitude. In Eq. (1), the axial components D_{xx}, C_{xx} are calculated by means of the permeability K and inertial constant J derived from the fit of experimental data using a porous medium model for the cable bundle friction in CICC [6]. For isotropic materials it is known that $C_{ij} = 1/K\delta_{ij}, D_{ij} = 2J/\sqrt{K}\delta_{ij}$, where δ_{ij} (= 1 if $i = j$ and = 0 otherwise) is the Kronecker delta. Although scattered data were reported in the past [6] on the radial components D_{rr} and C_{rr}, these are not considered very reliable [6]. Therefore, the anisotropy effect was taken into account here only by sensitivity studies, increasing arbitrarily by a factor 10 the values of D_{rr} and C_{rr} with respect to the axial components above. However, the computed effect on friction in the cable bundle region and heat transfer turned out to be not very significant, so that the results of this sensitivity study will not be reported here.

Two different models are considered here, which are discussed in more detail below:

- the periodic (P) model, see Fig. 2, which was the basis for the work in all papers [7–11] of this series so far;
- the non periodic (NP) model, which is needed in the case of net mass flow rate between annular region and central channel.

2.1. Periodic model

With the periodic model, see Fig. 2, the computational domain is obviously reduced to the minimum, i.e., a single period of the spiral, so that the computational cost is also minimized, at the expense of restricting the conditions that can be analyzed, e.g., no net mass flow is allowed through the spiral in this case, because this should violate the periodicity.

We impose the (axial) pressure drop Δp over the CICC length L (or the total axial mass flow rate $\dot{m}_{tot}$), the inlet bulk temperature $T_{in} = \int_{in} T(r)|\rho \mathbf{v} \cdot \mathbf{dA}| / \int_{in} |\rho \mathbf{v} \cdot \mathbf{dA}|$ and the heat source Q; the code calculates $\dot{m}_{tot}$ (or Δp), the outlet bulk temperature $T_{out} = \int_{out} T(r)|\rho \mathbf{v} \cdot \mathbf{dA}| / \int_{out} |\rho \mathbf{v} \cdot \mathbf{dA}|$ and the mass flow rate repartition between bundle region and hole.

From the mathematical point of view, periodicity is guaranteed by enforcing periodic boundary conditions at the *in-out boundaries*, see Fig. 2, for the flow velocity $\mathbf{v}$, the turbulent kinetic energy k, the turbulent dissipation rate ε, the normalized temperature θ and the pressure modulation $\tilde{p}$, where the pressure field is written as:

$$p = \tilde{p} + \beta \cdot x, \quad \text{where } \beta = \Delta p / L \tag{2}$$

and the temperature field is normalized as:

$$T = \theta + \sigma \cdot x, \quad \text{where } \sigma = Q/(\dot{m} C_p L) \tag{3}$$

where C_p is the specific heat at constant pressure.

The rest of the boundary conditions is chosen as follows:

- On the walls:
  - $v = 0$
  - $\partial k/\partial n = \partial p/\partial n = 0$
  - $\partial T/\partial n = 0$ (adiabatic outer wall) or temperature and heat flux continuity between solid and fluid (internal spiral wall) for the energy equation.
- At the symmetry axis ($r = 0$): $\partial \phi/\partial r = 0, \forall \, scalar \, \phi$
- At the interface between porous medium and central channel: continuity of the superficial (seepage) velocity components, i.e., the velocity derived from the volumetric flow rate on the domain considered free from any solid matrix blockage, to guarantee mass conservation.

2.2. Non periodic model

In this case a length of conductor consisting of several (tens of) spiral pitches is considered. Since the periodicity assumption is relaxed, we can study with this model also the relevant case of net mass flow between the two regions. The conductor is typically fed at the inlet section with the fully developed flow distribution resulting from the periodic model.

With the non periodic model we can also treat the case of temperature dependent thermophysical properties[1] which is obviously relevant in cryogenic conditions but is not tractable by the periodic model.

When a heated section is present, the domain extends for several pitch lengths downstream of the heated section, such as to allow a proper (averaged) analysis of the effects of the heating in a non-directly perturbed region.

3. Transverse mass transfer

We now come to the results of the model and address first the question of transverse mass transfer between cable bundle region and central channel.

As already noted elsewhere [6], this is by far the least investigated and perhaps least understood of all radial transport mechanisms in

[1] The only exception is C_p, which is assumed constant in the FLUENT porous medium model [13].

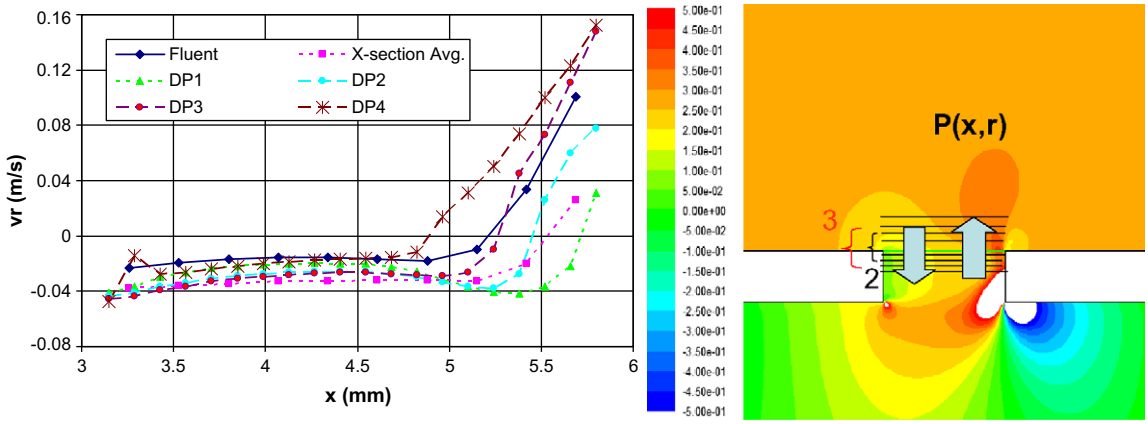

Fig. 3. Computed radial flow and pressure fields for $g/h = 2.7$. (a) Axial distribution of the computed transverse (radial) flow in the gap, at the interface between central channel and bundle region: FLUENT (solid line) vs. classical correlation Eqs. (4) and (5). Different symbols correspond to cross-section average or different distances from the interface taken as reference for the transverse pressure drop; the interface is conventionally taken as the surface of area $Ar = \pi(Din + 2h)g$. $\Delta p1$ to $\Delta p4$ correspond to pressure drop measured at 0.25 mm, 0.5 mm, 0.75 mm and 1 mm distance, respectively, across the interface. (b) Relative pressure field (Pa) and location of the surfaces to be used for the reference pressure drop in the radial flow correlation Eqs. (4) and (5). The arrows indicate the direction of the (re-circulating) transverse flow through the interface. The main (axial) flow is from left to right. (For interpretation of the references to colour in this figure legend, the reader is referred to the web version of this article.)

the CICC, direct evidence of it being restricted to basically a single paper [14].

Let us address the problem by using first the periodic model. In this case, although we cannot have a net transverse mass flow through the perforation as seen above, we can still have a local transverse flow averaging to zero. Also, there is no heat source in this case to pressurize selectively one of the two CICC regions, so that the driver of the local transverse flow can only be intrinsic and due to pressurization in front of the downstream wall of the gap, see below. In Fig. 3a the computed radial flow distribution on the interface (bottom or ceiling of the gap) between central channel and annular bundle region is shown, together with the results of the standard correlation presently used in 1D codes, i.e., [2]

$$v_r = sign(\Delta p)\sqrt{\frac{2|\Delta p|}{\rho}} \tag{4}$$

$$\Delta p = p_H - p_B, \quad sign(\Delta p) \equiv \Delta p/|\Delta p| \tag{5}$$

While in global 1D codes the fluid in the entire region is characterized by a single pressure, as the 1D model results from averaging over the other two coordinates, here different distances from the interface are taken as reference for the computation of the local Δp, and compared also with the respective cross-section average at constant x in bundle and hole.

The radial flow profile computed by FLUENT is in qualitative agreement with the classical scaling, giving (at zero net mass flow) a flow from bundle to hole in the upstream part of the gap, followed by a flow re-circulating back from hole to bundle region. This pattern is related to the pressure field as computed by FLUENT, see Fig. 3b, used in input for the standard correlation results, and in particular to the pressurization in front of the downstream wall of the gap, which was already highlighted in the previous papers of this series as responsible for the (form) friction effect in the central channel.

In order to develop a bit further the question of the correlation between the radial mass flux $\Gamma = \rho v_r$ and Δp, let us reconsider the same problem as above, by using now the non periodic model. This allows us to have a net mass flow between bundle region and central channel. Furthermore, three different axial mass flow rates $\dot{m}_{tot} = 4$, 7 and 10 g/s are considered with heating power $Q = 100$ W distributed over one pitch length; two different heating powers Q (50 W and 100 W) were also considered to check the effect of Q (for the 4 g/s case only), which however results to be negligible, see Fig. 4.

If we use as relevant Δp the volume average $\langle \Delta p \rangle$ "above" and "below" the gap in each pitch length, we see in Fig. 4 that the radial volume flow rate $\dot{m}_r/\rho = \Gamma A_r/\rho = v_r A_r$ correlates quite well, albeit now *quadratically*, with $\langle \Delta p \rangle$, the more so the larger the axial mass flow rate. However, a significant offset, also depending on the operating conditions, is present, implying that a finite $\langle \Delta p \rangle$ is compatible with $\Gamma \sim 0$, which seems in contradiction with the simple correlation (4) implemented at present in the 1D global models.

However, as it can be seen from Fig. 3, a significant perturbation of the pressure profile can be present even in the absence of net transverse mass flow, and this perturbation increases with $\dot{m}$; this suggests to try and subtract from $\langle \Delta p \rangle$ the volume average $\langle \Delta p_0 \rangle$ obtained above in the case of the periodic model. The result is shown in Fig. 5, where the offset which was present in Fig. 4 indeed practically disappeared. It may therefore be argued that, if we want to establish a correlation between the global 1D model assumptions on Γ and the local 2D results obtained by FLUENT, then the relevant quantity should be the *reduced* pressure difference $\langle \Delta p \rangle - \langle \Delta p_0 \rangle$. In Fig. 5, however, a $\dot{m}$ dependence is still present, so that we cannot obtain a general correlation for Γ, valid for all $\dot{m}$, at this time.

4. Transverse momentum transfer – effect of the perforation on friction

Since the pressure distribution in the cable bundle region is not significantly perturbed by the presence of the perforation, see Fig. 3b, the effect of the perforation on the bundle friction factor f_B is modest and we can concentrate here on the effect of the perforation on the friction factor in the central channel, f_H.

At first sight, see Fig. 6, it could seem that the strong modification of the streamlines introduced by the perforation should imply a significant change in f_H. However, if one considers, for the same $g/h = 2.7$ peculiar, e.g., of the CSMC conductor, the radial distribution of the Δp between the vertical walls of the gap, which is responsible for the dominating (form) friction contribution, we see in Fig. 7a that the distributions with and without perforation are quite close to each other on average, resulting (for Reynolds number in the central channel $Re_H \sim 1.4 \times 10^5$) in $f_H \sim 9.9 \times 10^{-3}$ for the impermeable case whereas $f_H \sim 9.7 \times 10^{-3}$ for the permeable case.

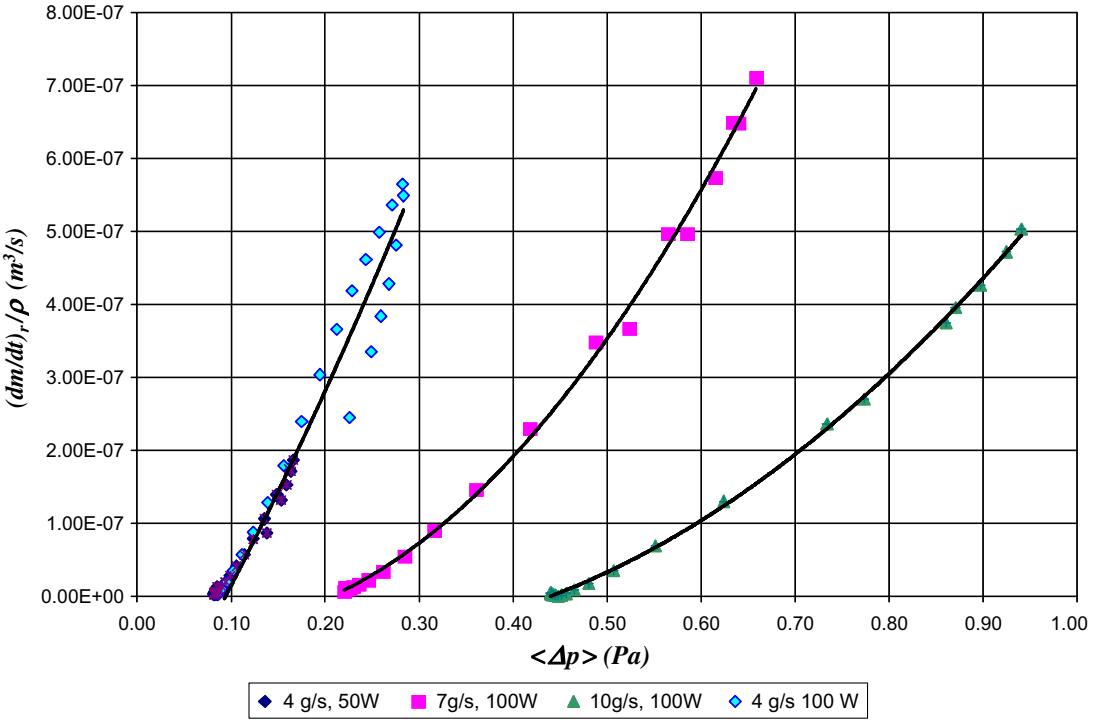

Fig. 4. Volumetric radial mass flow rate $(dm/dt)_r$ vs. volume averaged radial pressure drop for different total (axial) mass flow rates and heating powers (symbols), with the corresponding quadratic fits (lines). (For interpretation of the references to colour in this figure legend, the reader is referred to the web version of this article.)

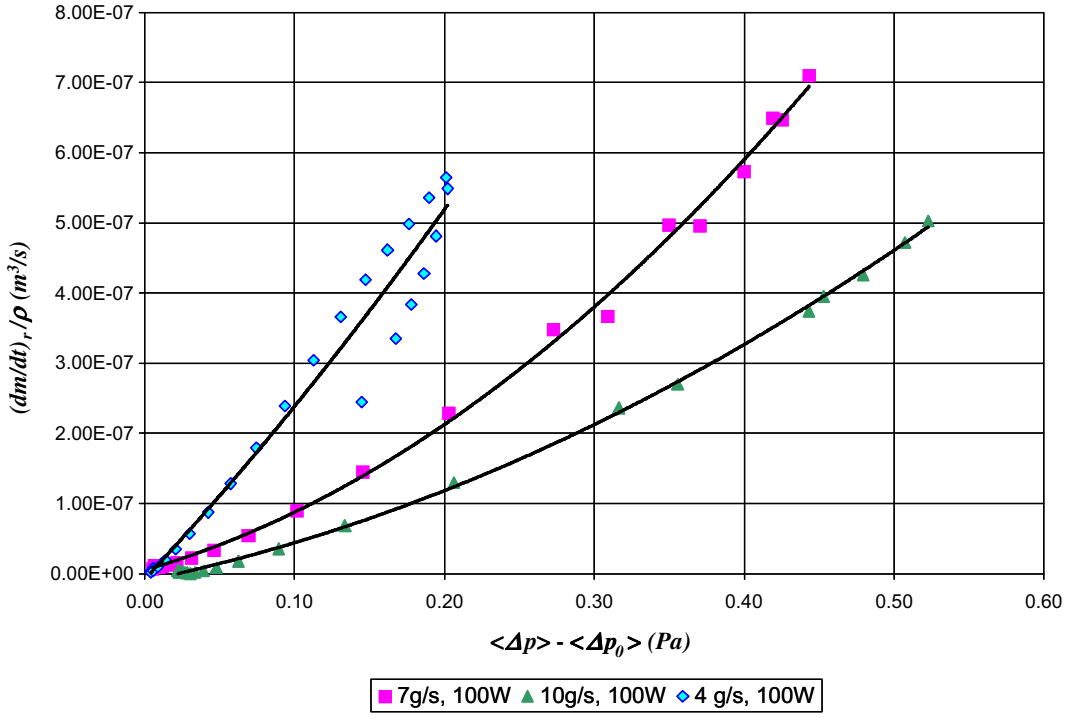

Fig. 5. Volumetric radial mass flow rate $(dm/dt)_r$ vs. *reduced* radial pressure drop for different total (axial) mass flow rates and heating powers (symbols), with the corresponding quadratic fits (lines). (For interpretation of the references to colour in this figure legend, the reader is referred to the web version of this article.)

Since for $g/h = 2.7$ a wide experimental database is available, the results of the FLUENT calculation are compared in Fig. 8 with the measurements done by different authors in different operating conditions [15–16]. It is seen that the CFD results (obtained with different models and fluids) are always within at most 20% error bar of the experimental data, which have, in turn, their rather significant spread, depending also on the operating conditions of the tests.

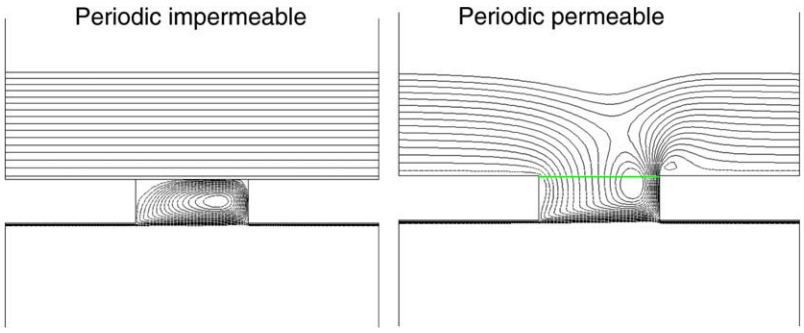

Fig. 6. Computed streamlines in the periodic impermeable case (left) and periodic permeable case (right), $g/h = 2.7$.

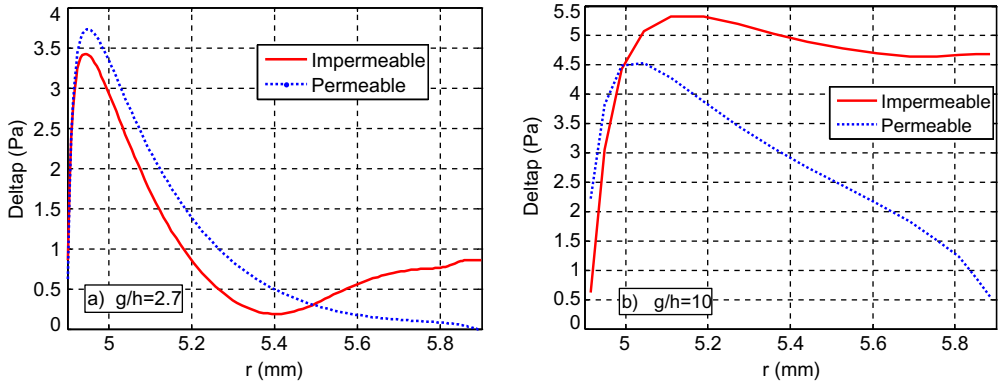

Fig. 7. Radial distribution of the axial pressure drop in the gap using the permeable (dotted, blue line) or the impermeable (solid, red line) model. (a) $g/h = 2.7$ and (b) $g/h = 10$. (For interpretation of the references to colour in this figure legend, the reader is referred to the web version of this article.)

The picture just presented changes however quite dramatically if we now consider a larger gap width, e.g., $g/h = 10$, see Fig. 9. In this case the flow in the central channel has sufficient room to reattach at the bottom of the gap in the impermeable case and this reflects directly both on the (relatively flat) pressure profile on the downstream wall of the gap (see Fig. 7b) and on the core flow of the central channel. Therefore, the permeable interface offers in this case a better opportunity than in the case $g/h = 2.7$ for a relief of the pressurization on the downstream edge of the spiral, thus leading to a significant reduction of the friction factor.

It may also be interesting to note that in this case the standard experimental procedure[2] for the measurement of f_H, which implicitly assumes that the perforation plays no role, should *not* be supported by the present calculation. Indeed, for a large gap the difference in flow in the central channel between the cases with and without perforation appears on the contrary to be significant.

5. Transverse heat transfer between bundle region and central channel – effect of the perforation

We now move to the final part of our discussion of the CFD model results by considering the question of heat transfer. While the (limited) enhancement in the heat transfer on the side of the central channel due to the presence of the spiral was already considered in a previous paper of this series [11], we concentrate here on the effect of the perforation on the heat transfer between the two CICC regions. For that purpose we use the non periodic model described above, applying a power Q on a single pitch length in the bundle region.

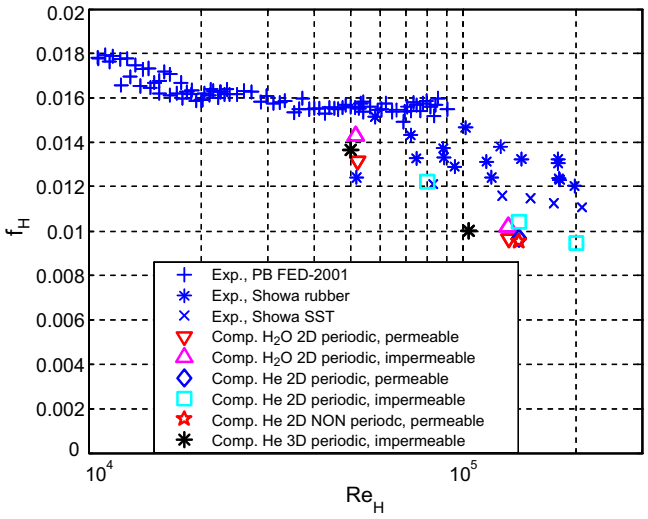

Fig. 8. Comparison between measured and computed friction factors in the central channel with $g/h = 2.7$, as a function of the Reynolds number.

The results of a typical computation are shown in Fig. 10. We note from the 2D temperature profile that the heat progressively penetrates from the bundle region to the central channel. A zoom of the 2D isotherms in the gap region, for the pitches just downstream of the source, is shown in Fig. 11: it is seen that while in

[2] The standard experimental procedure goes either through the derivation of the mass flow rate in the central channel, assuming it is equal to the difference between the total mass flow rate and the mass flow rate measured by plugging the central channel [15], or else through the measurement of the friction factor in spiral rib-roughened tubes, assuming it is equal to that of the central channel [16].

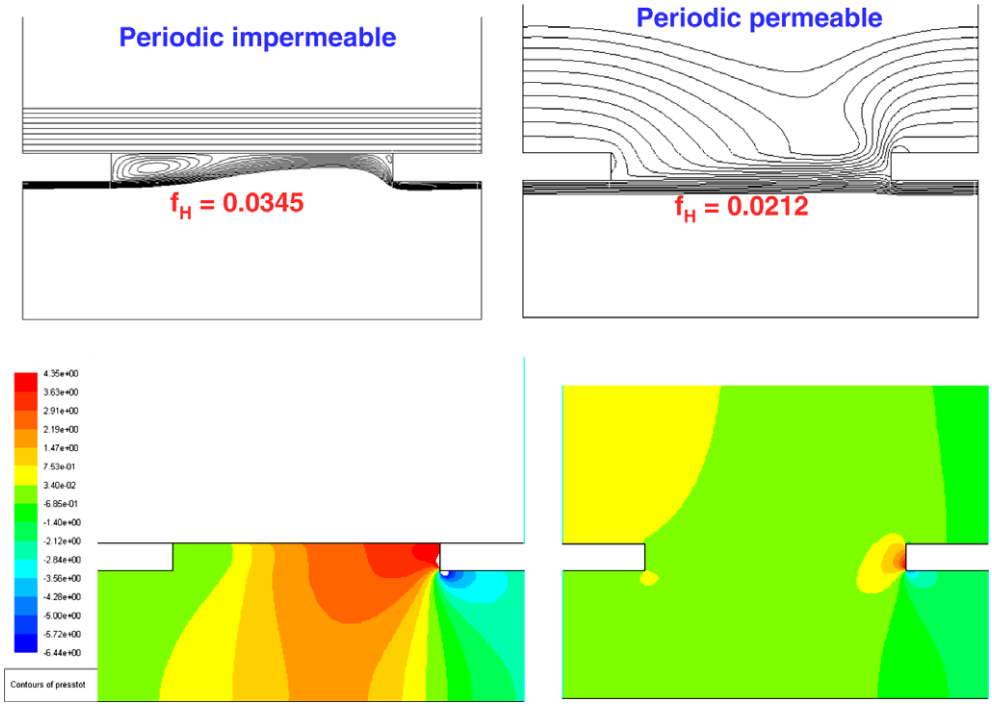

Fig. 9. Case $g/h = 10$. Computed streamlines (top) and corresponding relative pressure distribution (bottom, Pa) in the periodic impermeable (left) and periodic permeable (right) case.

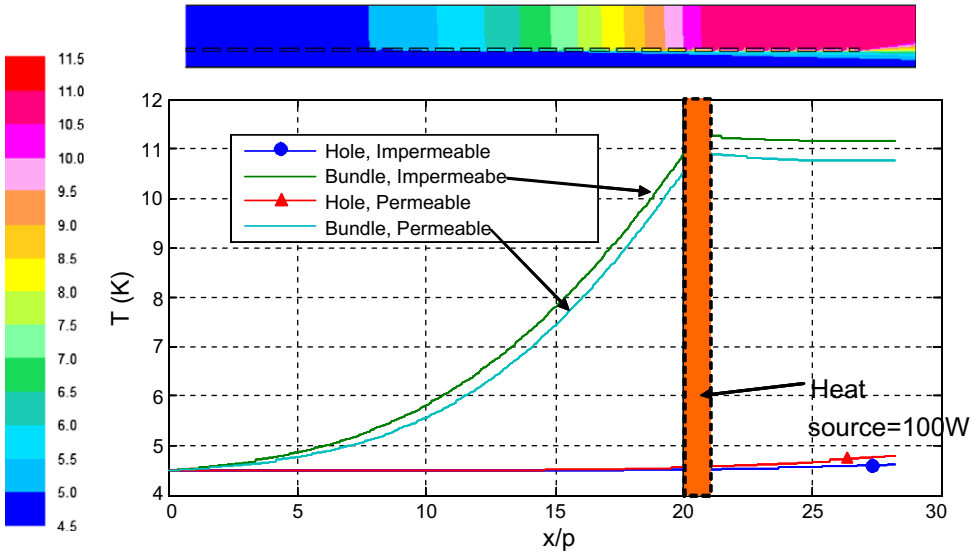

Fig. 10. Computed 2D temperature distribution (top) and axial temperature profiles at $r = 19.5$ mm in the bundle region (bundle = outer boundary) and at $r = 0$ mm (hole = central channel axis) in the hole, for both permeable and impermeable case, at 7 g/s total mass flow rate. The abscissa is normalized to the pitch length pt of the spiral.

the impermeable case the heat is conducted across the gap, and the heat transfer is enhanced by re-circulation, in the permeable case the hot bundle fluid penetrates the gap, so that the heat is also advected by the transverse mass flow in this case.

The axial temperature profiles at the outer boundary of the cable bundle region and on the axis of the central channel are also compared in Fig. 10, for the cases of permeable and impermeable interface. It is seen that the profiles are similar, with comparable temperature differences. However, the resulting heat fluxes $Q_{B\to H}$, sum of the advection heat flux through the gap (for the permeable case) and the conduction heat flux through the spiral and gap, are very different in the two cases, so that the computed heat transfer coefficient:

$$H_{BH} = Q_{B\to H}/(T_B - T_H) \tag{6}$$

increases by a factor of 2–5 in the permeable case, see Fig. 12.

In Fig. 12 the results of the FLUENT computation are also compared with the range of values coming from measurements recently performed at CRPP Villigen, Switzerland [17]. It is seen that the CFD model reproduces within a factor of ~2 the measured range of values (which was however derived for a slightly different

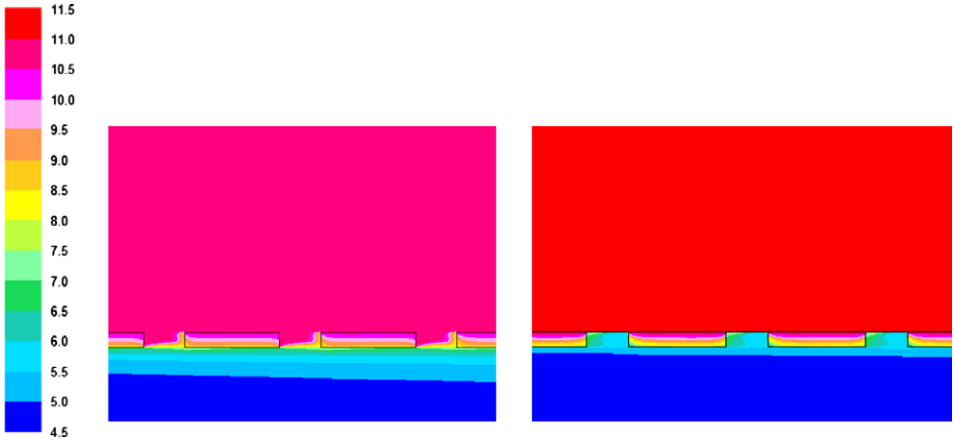

Fig. 11. Zoom of the computed 2D temperature distribution (K) in the CICC region downstream of the heat source: permeable case (left) vs. impermeable case (right).

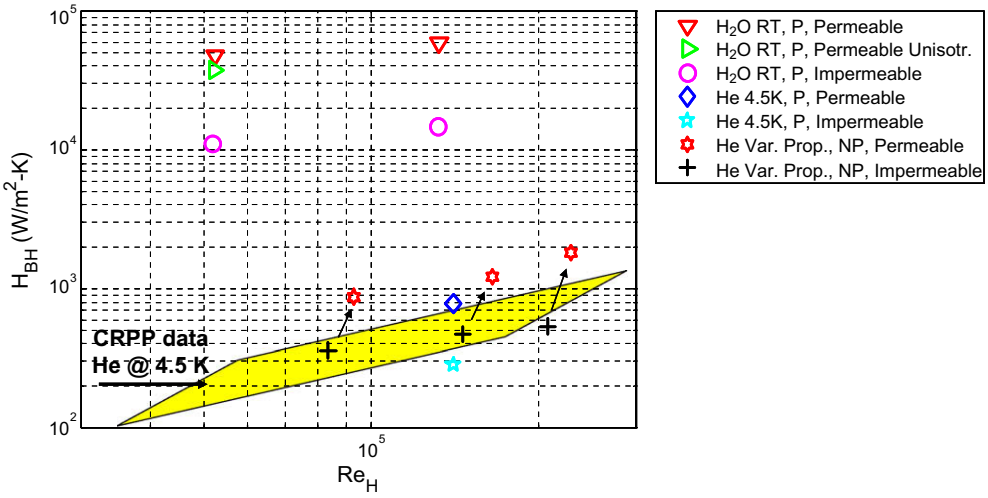

Fig. 12. Comparison of computed (different symbols) and measured (trapezoidal region) heat transfer coefficients.

CICC, with respect to the one considered here, compare Table 1 and [17]).

6. Conclusions and perspective

The recently developed CFD model of an ITER CICC, limited so far to an isolated central channel or to the simplest cable bundle, has been extended to include the effects of a permeable interface between central channel and cable bundle regions, as present in a real CICC.

The main results of this paper can be summarized as follows:

- The physical origin and relation between the transverse mass flux Γ and the transverse Δp has been discussed; the simple correlation used for Γ in global 1D codes is at least qualitatively supported by the CFD model.
- The permeable interface increasingly affects the friction factor f_H in the central channel at increasing g/h; computed values of f_H are within 20% of experimental values; at larger g/h the experimental procedure which is customarily used for the measurement of f_H should become questionable, as it neglects the perforation.
- The permeable interface significantly affects the heat transfer coefficient H_{BH} between cable bundle region and central channel: H_{BH} is much larger, by a factor 2–5, in the case of permeable interface; the computed H_{BH} values are within a factor of 2 from the experimental range.

Table 1
Geometrical data of the CICC considered in the simulations (all in mm).

	g	h	w	pt	D_{in}	D_{Jk}
$g/h = 2.7$	2.7	1	6.25	8.95	9.8	39
$g/h = 10$	10			16.25		

Correlations for transverse heat and mass transfer, aimed at feeding constitutive relations for the global 1D models, could be derived from a systematic/comprehensive application of the local 2D CFD analysis presented here, covering parametrically the relevant space of Reynolds and Prandtl numbers.

References

[1] Mitchell N, Bessette D, Gallix R, Jong C, Knaster J, Libeyre P, et al. The ITER magnet system. IEEE Trans Appl Supercond 2008;18:435–40.
[2] Zanino R, DePalo S, Bottura L. A two-fluid code for the thermohydraulic transient analysis of CICC superconducting magnets. J Fus Energy 1995;14:25–40.
[3] Savoldi L, Zanino R. M&M: multi-conductor Mithrandir code for the simulation of thermal–hydraulic transients in superconducting magnets. Cryogenics 2000;40:179–89.
[4] Savoldi Richard L, Bagnasco M, Zanino R. Multi-solid multi-channel Mithrandir (M3) code for thermal–hydraulic modelling of ITER cable-in-conduit superconductor. Fus Eng Des 2007;82:1607–13.

[5] Zanino R, Bagnasco M, Fillunger H, Heller R, Savoldi Richard L, Suesser M, Zahn G. Thermal–hydraulic issues in the ITER toroidal field model coil (TFMC) test and analysis. Adv Cryo Eng 2004;49:685–92.
[6] Zanino R, Savoldi Richard L. A review of thermal–hydraulic issues in ITER cable-in-conduit conductors. Cryogenics 2006;46:541–55.
[7] Zanino R, Giors S, Mondino R. CFD modeling of ITER cable-in-conduit superconductors. Part I: friction in the central channel. Adv Cryo Eng 2006;51:1009–16.
[8] Zanino R, Giors S, Mondino R. CFD modeling of ITER cable-in-conduit superconductors. Part II: effects of spiral geometry on the central channel pressure drop. Fus Eng Des 2006;81:2605–10.
[9] Zanino R, Giors S, Savoldi Richard L. CFD modeling of ITER cable-in-conduit superconductors. Part III: correlation for the central channel friction factor. In: Proceedings of the 21th international cryogenic engineering conference (ICEC21), vol. 1; 2007. p. 207.
[10] Zanino R, Giors S. CFD modeling of ITER cable-in-conduit superconductors. Part IV: friction factor of the simplest (triplet) bundle. In: Proceedings of the 21th international cryogenic engineering conference (ICEC21). vol. 1; 2007. p. 201.
[11] Zanino R, Giors S. CFD modeling of ITER cable-in-conduit superconductor. Part V: combined momentum and heat transfer in rib roughened pipes. Adv Cryo Eng 2008;53:1261–8.
[12] Chen HC, Patel VC. Near-wall turbulence models for complex flows including separation. AIAA J 1988;26:641–8.
[13] Fluent 6.3 User's Guide. Lebanon (NH): Fluent Inc.; 2006.
[14] Shatil N, Zhelamskij M, Anghel A, Vecsey G, Takahashi Y, HamadaK. The first experimental observation of the He mass exchange between cable space and central channel in CICC obtained by SHF method during QUELL. In: Proceedings of the 20th symposium on fusion technology; 1998. p. 715–8.
[15] Bruzzone P. Pressure drop and helium inlet in the ITER CS1 conductor. Fus Eng Des 2001;58–59:211–5.
[16] Nicollet S, Duchateau JL, Fillunger H, Martinez A, Parodi S. Dual channel cable in conduit thermohydraulic: influence of some design parameters. IEEE Trans Appl Supercond 2000;10:1102–5.
[17] Marinucci C, Bottura L, Bruzzone P, Stepanov B. Analysis of transverse heat transfer coefficients in a dual channel ITER-type cable. Cryogenics 2007;47:563–76.